ADVANCING EARTH AND SPACE SCIENCES

Geophysical Research Letters

RESEARCH LETTER
10.1029/2026GL125170

Evaluating the Role of Kernel Choice on Radiative Feedback Estimates

Kaitlyn Wen[1], Ivan Mitevski[2], Tyler P. Janoski[3,4,5,6], and Gabriel A. Vecchi[2,7]

[1]Department of Computer Science, Princeton University, Princeton, NJ, USA, [2]Department of Geosciences, Princeton University, Princeton, NJ, USA, [3]Department of Environmental Sciences, Rutgers University, New Brunswick, NJ, USA, [4]The City College of the City University of New York, New York, NY, USA, [5]NOAA-CESSRST-II, The City College of the City University of New York, New York, NY, USA, [6]NOAA/OAR National Severe Storms Laboratory, Norman, OK, USA, [7]High Meadows Environmental Institute, Princeton University, Princeton, NJ, USA

Key Points:

- Kernel choice causes meaningful spread across water vapor, albedo, and cloud feedbacks in the polar regions
- An important factor in interkernel spread is the base climate state used to derive the kernels
- Feedback decomposition residuals span a consistent intermodel range of ~0.7 Wm^{-2} regardless of the kernel applied

Supporting Information:

Supporting Information may be found in the online version of this article.

Correspondence to:

I. Mitevski,
mitevski@princeton.edu

Citation:

Wen, K., Mitevski, I., Janoski, T. P., & Vecchi, G. A. (2026). Evaluating the role of kernel choice on radiative feedback estimates. *Geophysical Research Letters*, *53*, e2026GL125170. https://doi.org/10.1029/2026GL125170

Received 22 JUN 2026
Accepted 22 AUG 2026

Abstract Radiative feedbacks are important for understanding climate sensitivity, yet estimates vary widely across climate models. Feedbacks are often computed using the radiative kernel technique, which uses pre-calculated radiative sensitivities (kernels) derived from different models and base states. While much attention has been given to intermodel differences, the impact of kernel choice has received less scrutiny. Here, we quantify the influence of 10 radiative kernels on feedback estimates from 48 CMIP5 and CMIP6 models. We find that kernel-related spread is comparable to the intermodel spread in global water vapor and albedo feedbacks, and in polar regions, the kernel-induced spread for cloud feedbacks is also comparable to the model spread. We show that differences in the base climate state used to derive kernels are an important source of this spread. Our results suggest that we should account for uncertainties due to kernel choice, particularly in polar amplification studies.

Plain Language Summary Understanding how much the Earth will warm in response to increasing greenhouse gases depends in part on "radiative feedbacks"—processes that can amplify or dampen climate change. We often estimate these feedbacks using a method called the radiative kernel technique, which relies on pre-computed tools known as kernels. However, different research groups use different kernels, and it has not been clear how much this choice affects the feedback results. In this study, we applied 10 different kernels to climate model simulations from two major climate model archives to measure how much the choice of kernel influences estimates of radiative feedbacks. We found that the uncertainty from using different kernels is comparable to the spread typically seen between different models in the polar regions. Our results suggest that we should be careful about kernel choice when studying radiative feedbacks, especially for topics like polar amplification.

1. Introduction

Given a certain radiative forcing from greenhouse gases in the atmosphere, how much near-surface warming should we expect? This fundamental quantity in climate science, known as the "climate sensitivity," serves as the basis for our confidence in future climate projections. Decades of work have gone into better constraining estimates of climate sensitivity (Charney et al., 1979; Sherwood et al., 2020), but a wide range of values persists. Although there is some uncertainty regarding the forcing from CO_2 (He et al., 2023; Mitevski et al., 2025), this is largely a result of persistent uncertainty in radiative feedbacks that act to amplify or dampen the initial temperature response to radiative forcing; therefore, better constraining radiative feedbacks will likely reduce uncertainty in climate sensitivity estimates and better inform assessments of future climate risk.

Although there are different "flavors" of climate sensitivity, the most ubiquitous metric is the equilibrium climate sensitivity (ECS): the global near-surface temperature increase at equilibrium after doubling atmospheric CO_2 levels from preindustrial levels. Efforts to constrain ECS date back to the Charney Report in 1979 (Charney et al., 1979), which estimated the likely range of ECS to be between 1.9 and 5.2 K. More recent assessments, synthesizing current understanding of feedback processes as well as historical and paleoclimate records, estimated a likely (66%) range of 2.6–3.9 K (Sherwood et al., 2020).

The ECS is often approximated as the effective climate sensitivity (EffCS). EffCS is calculated from climate model simulations where the atmospheric CO_2 is abruptly doubled from a long, equilibrated preindustrial run, after which the model is integrated for several hundred years. The net top-of-atmosphere (TOA) radiative imbalance ΔN due to CO_2 doubling is linearized as

$$\Delta N = F + \lambda \Delta T, \tag{1}$$

where F represents the radiative forcing from the CO_2 increase, λ is the net feedback parameter, and ΔT is the global mean surface temperature change due to the imposed forcing F. A linear regression is performed with the "independent" variable ΔT and the dependent variable ΔN to estimate the y-intercept F and the slope λ. Most of the uncertainty in estimating EffCS arises from the feedback parameter λ (Sherwood et al., 2020), with a smaller contribution from the radiative forcing F (Soden et al., 2018).

The net feedback parameter λ can be linearly decomposed into individual feedbacks representing distinct climate processes: $\lambda = \sum_i \lambda_i$. Each λ_i is one of the major feedbacks: the lapse rate (LR), Planck, water vapor, surface albedo, or cloud feedbacks. The most common method for decomposing λ in this way is with radiative kernels (Soden et al., 2008). Radiative kernels are pre-calculated radiative sensitivities to incremental changes in climate state variables, expressed as $\frac{\partial R_i}{\partial x_i}$, where R_i is the net TOA radiative flux and x_i denotes variables such as temperature, water vapor, and surface albedo (Soden & Held, 2006). For further technical details regarding radiative kernel analysis, see Janoski et al. (2025).

Despite widespread use of radiative kernels, the spread in λ_i due to kernel choice is underexplored compared to the spread due to climate model choice. Zelinka et al. (2020) examined global average feedbacks with six radiative kernels and determined that the qualitative results were not kernel-dependent, but did not go so far as to explicitly compare interkernel to intermodel spread. Recent polar amplification studies have noted large discrepancies, especially in polar regions: Hahn et al. (2021) showed that the albedo and cloud feedbacks in the Arctic and Antarctic exhibit substantial spread across six different kernels; Donohoe et al. (2020) found significant variability in the sea-ice albedo feedback; and H. Huang and Huang (2023) reported an interkernel spread exceeding 30% in polar regions, attributing this to the differences in the base states used to derive the kernels.

As the collection of radiative kernels continues to grow, and different studies use different kernels, there is a need to quantify the spread in feedbacks due to kernel choice (interkernel spread) and compare it to the spread arising from the use of different models (intermodel spread). Here, we investigate the interkernel spread across 48 models from the Coupled Model Intercomparison Project Phase 5 and 6 archives by computing the Planck, LR, water vapor, albedo, and cloud feedbacks using 10 radiative kernels. Then, we quantify the interkernel and intermodel spread for global, Arctic, and Antarctic average feedback values. Finally, we compare the residuals from each kernel to the intermodel spread in feedbacks.

2. Methods

We analyzed output from fully coupled atmosphere-ocean-sea-ice-land model experiments in which atmospheric CO_2 concentrations are abruptly quadrupled from a long preindustrial control run and held fixed for 150 years. The response is defined as the difference between the $4\times CO_2$ run and the time-averaged preindustrial control run monthly climatology. We utilized output from 48 climate model experiments from the fifth and sixth phases of the Coupled Model Intercomparison Project (CMIP5 and CMIP6). A complete list of the CMIP5 and CMIP6 models is in Table S1 in Supporting Information S1. We note that these 48 models do not represent strictly independent estimates, as multiple modeling centers contributed structurally related versions to both the CMIP5 and CMIP6 archives.

To compute feedbacks, we follow the commonly used Gregory approach (Chung & Soden, 2015; Huo et al., 2024; Zhang et al., 2018, 2020). Radiative feedbacks are calculated with the ClimKern v1.2 Python package (Janoski et al., 2025) by convolving simulated variable responses from each month of the 150-year-long $4\times CO_2$ simulation with corresponding radiative kernels. The applicable longwave (LW) or shortwave (SW) TOA radiative perturbation (ΔR_i) is computed for each feedback: Planck, LR, water vapor, albedo, and cloud. Then, the resulting TOA radiative perturbations are annually averaged and linearly regressed onto the global-average surface skin temperature response (ΔT), as in Gregory et al. (2004); the feedback (λ_i) is estimated as the slope of the regression. The net TOA radiative flux response is similarly regressed to obtain the net feedback parameter (λ), which is used to calculate the residual in the global energy budget.

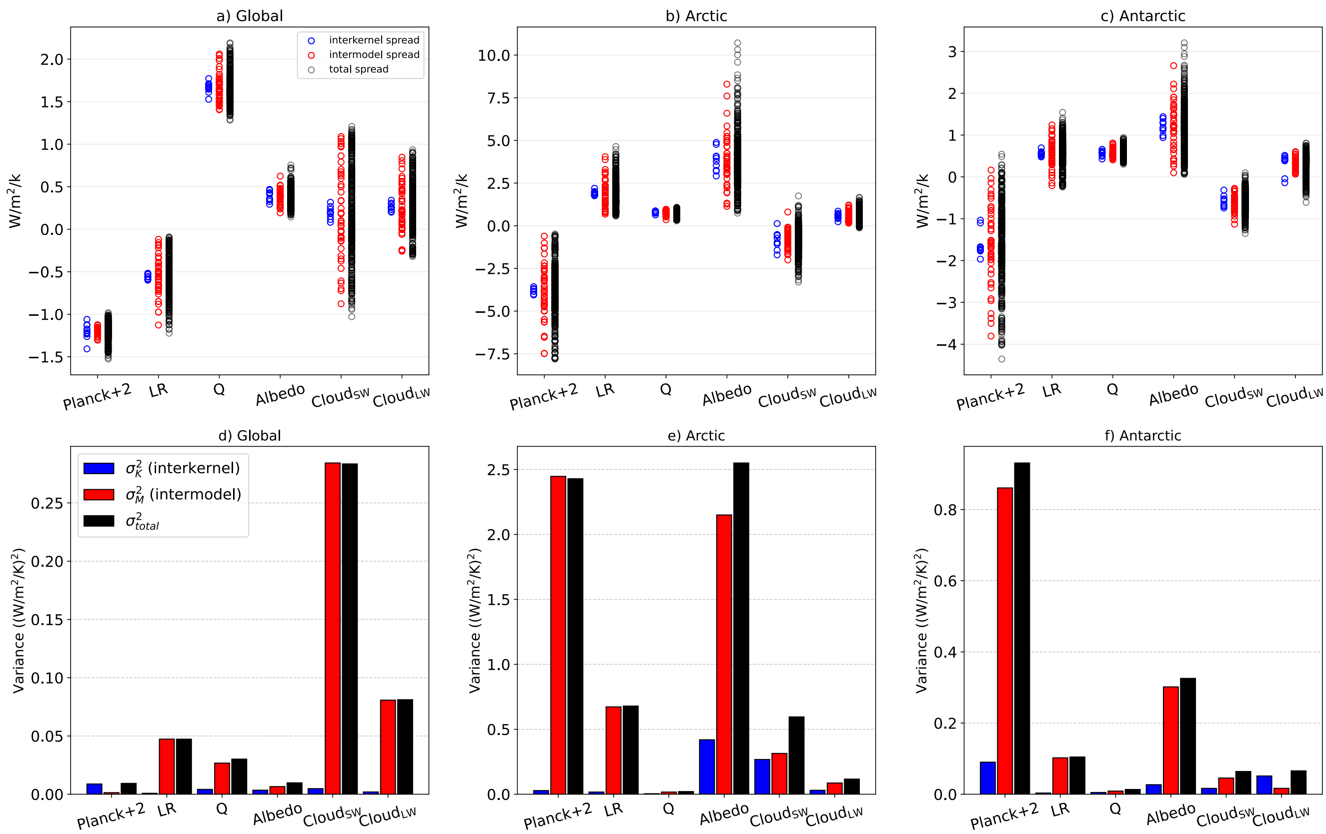

Figure 1. Planck, lapse rate, water vapor, albedo, and shortwave and longwave cloud feedbacks for interkernel (blue), intermodel (red), and all model–kernel combinations (black). Feedbacks are shown for (a) global, (b) Arctic, and (c) Antarctic regions. The interkernel spread is represented by 10 points (one per kernel), each averaged over all 48 models. The intermodel spread includes 48 points (one per model), each averaged over the 10 kernels. The total spread comprises 480 points (10 kernels × 48 models), representing all model–kernel pairs. For the variance estimators in panels (d–f) (also on same y-scaling in Figure S1 in Supporting Information S1), σ_M^2 represents the intermodel variance calculated across the model means; σ_K^2 is the interkernel variance calculated across the kernel means; and σ_{total}^2 is the total variance of the flattened grid of all model–kernel cells. The Arctic is defined as 70°N–90°N and the Antarctic as 70°S–90°S.

This process is repeated with 10 unique kernel sets provided by the ClimKern kernel repository (Janoski et al., 2025). ClimKern is an open-source Python library and data set for calculating radiative feedbacks in a standardized, reproducible way. For each model, we apply ClimKern functions to calculate feedbacks for temperature (Planck and LR), water vapor (Q), surface albedo, and clouds using each of the 10 kernels. We use the default tropopause definition for vertically integrating the temperature and water vapor feedbacks, which assumes a 300 hPa tropopause at the equator that decreases linearly with the cosine of latitude to 100 hPa at the poles. The water vapor feedback is calculated using method 1 in ClimKern. Rather than approximating the relative change in moisture as a simple fraction, this method computes the logarithmic difference in specific humidity to better capture its radiative scaling (see Janoski et al. (2025) for more details). The cloud feedback is divided into LW and SW components and calculated using the adjustment method (Soden et al., 2008). In total, there are 480 model–kernel pairs (48 models × 10 kernels).

To quantify the spread in radiative feedbacks due to differences in kernels—the interkernel spread—we average results across all 48 models for each kernel, yielding one value per kernel (10 in total). To quantify the spread due to differences among models—the intermodel spread—we average over the 10 kernels for each model, yielding one value per kernel (48 in total). To compare the relative magnitude of the interkernel and intermodel spreads, we calculate the variance across model means $\left(\sigma_M^2\right)$, kernel means $\left(\sigma_K^2\right)$, and total variance of all model-kernel combinations $\left(\sigma_{\text{total}}^2\right)$. Please note that we ignore the interaction term in the variance decomposition.

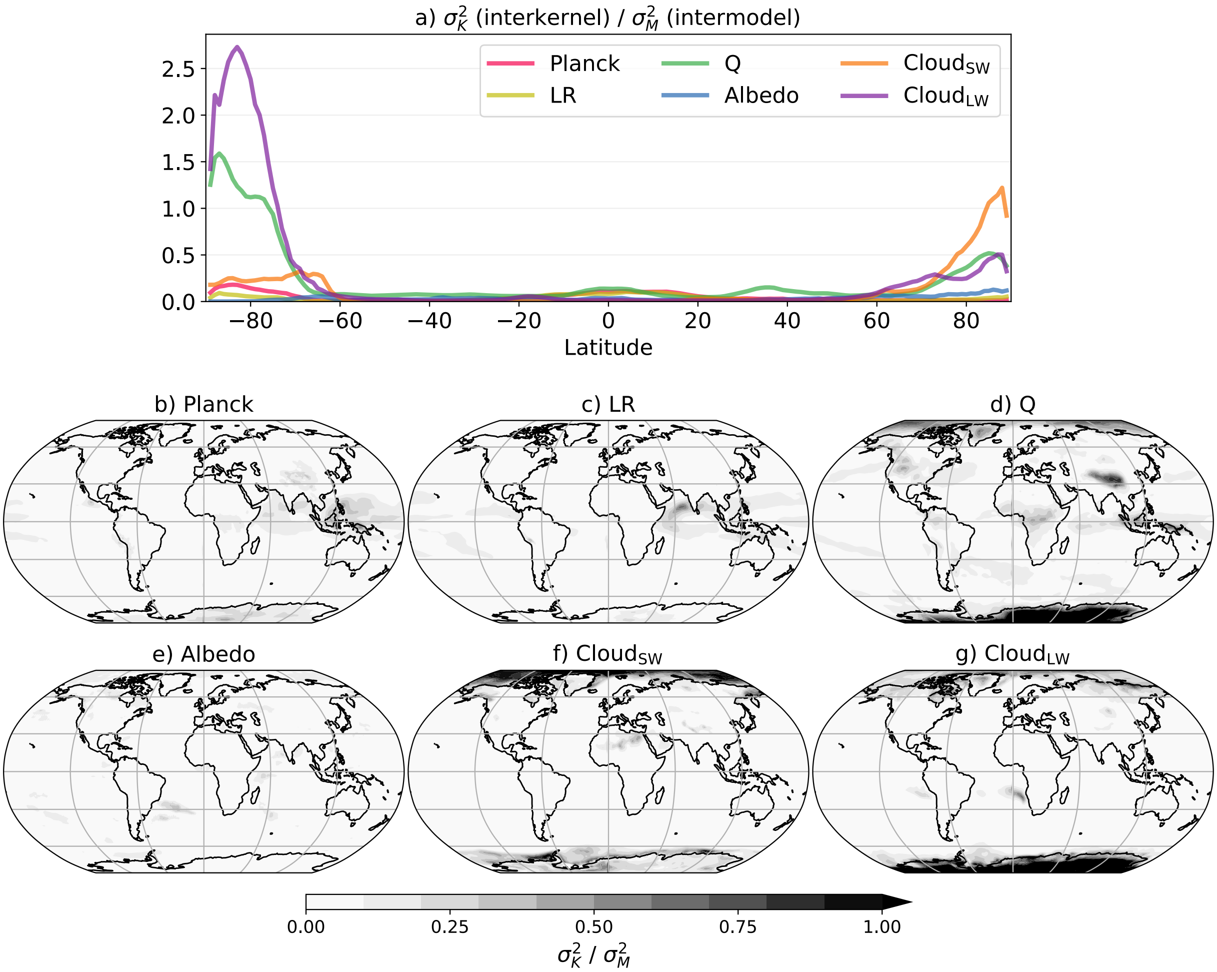

Figure 2. Ratio of interkernel to intermodel variance for (a) zonally-averaged feedbacks, and maps of (b) Planck, (c) lapse rate, (d) water vapor (Q), (e) surface albedo, (f) shortwave cloud, and (g) longwave cloud feedback spread ratios. For the interkernel spread, this range is calculated across 10 kernels, each averaged over 48 models. For the intermodel spread, the range is calculated across 48 models, each averaged over 10 kernels.

3. Results

We find that the interkernel spread (blue in Figure 1a) represents a meaningful fraction of the intermodel spread (red in Figure 1). To better quantify the spread from the kernels and models, we focus on σ_M^2, σ_K^2, and σ_{total}^2 in panels d, e, and f, respectively. For globally averaged feedbacks (d), interkernel variability is small relative to the overall intermodel spread. However, in the Arctic (e) and Antarctic (f) regions, the interkernel spread generally accounts for a larger fraction of the intermodel spread than in the global means. In the Arctic, albedo and cloud feedbacks exhibit considerable uncertainty due to interkernel spread, whereas in the Antarctic, the Planck and cloud feedbacks show substantial interkernel spread. For instance, the SW cloud feedback shows nearly equal interkernel and intermodel spread in the Arctic. Similarly, the LW cloud feedback in the Antarctic exhibits a larger interkernel spread comparable to the intermodel spread. This highlights the importance of accounting for kernel-related uncertainty when analyzing radiative feedbacks in the polar regions.

To quantify the importance of the interkernel to intermodel spread at all latitudes, we divide the zonal mean interkernel spread by the intermodel spread in Figure 2a. A ratio of 1 shows that the interkernel spread is as large as the intermodel spread, and a ratio of less than 1 shows that the interkernel spread is smaller than the intermodel spread. Similar to what we showed in Figure 1, the zonal interkernel spread is generally smaller than the intermodel spread in the lower latitudes; however, it becomes comparable to the intermodel spread in the polar regions for most feedbacks. Specifically, the albedo (blue), water vapor (green), and cloud (orange and purple) feedbacks show the strongest kernel dependence relative to model dependence in the poles, whereas the LR (gold) and

Planck (red) feedbacks have higher interkernel to intermodel ratios in the tropics. It is important to note that the interkernel to intermodel ratio is highest at the polar regions because both the interkernel spread is highest and the intermodel spread is lowest (see Figure S4 in Supporting Information S1).

The albedo feedback has the highest magnitude in the polar regions because of climatological sea ice, whose loss under a 4×CO_2 warming scenario enhances warming (Curry et al., 1995; Riihelä et al., 2021). As sea ice melts, the surface darkens, increasing the absorption of SW radiation and creating a positive (destabilizing) feedback. The regions with the highest sea-ice loss also show the highest interkernel spread (Figure 2d), indicating that the choice of kernel has its greatest influence in these areas. For instance, this ratio reaches 20% in the Southern Ocean and 40% in the Arctic. Other studies (e.g., Hahn et al., 2021) have also emphasized the significance of kernel selection when computing albedo feedbacks in polar amplification studies.

The SW cloud feedback also has high interkernel to intermodel spread ratios in the polar regions, with values approaching 1 in the Southern Ocean around 65°S and in the Arctic near 80°N (Figures 2a and 2e). Janoski et al. (2025) showed that part of this interkernel spread arises from the overlap between cloud and albedo feedbacks, particularly in regions where clouds coincide with sea ice, such as the Arctic and Southern Ocean. Previous studies (Hahn et al., 2021; H. Huang & Huang, 2023) have also reported substantial interkernel spread in cloud feedbacks, and others (Donohoe et al., 2020) have linked the large spread in albedo kernels in the Arctic and Southern Ocean due to the difference in mean-state cloudiness in the base state from which the kernels were derived. In contrast, interkernel spread is minimal in the tropics, where intermodel differences dominate. The small kernel-related uncertainty in this region suggests that kernel choice is unlikely to significantly affect observational constraints on climate sensitivity.

The water vapor and LW cloud feedbacks over Antarctica exhibit a large interkernel spread relative to the intermodel spread. Examining the spatial maps, we find the largest ratios over the Antarctic continent (Figure 2d). In the case of water vapor, the atmosphere over Antarctica contains very little moisture, so differences in the background state used to derive the kernels likely account for the substantial interkernel spread. Similarly, for the LW cloud feedback, most of the interkernel to intermodel spread ratio is concentrated over the Antarctic continent (Figure 2g).

In the tropics, we find the largest interkernel to intermodel ratio for Planck, LR, and water vapor feedbacks (Figure 2a and Figure S4 in Supporting Information S1), with considerable longitudinal variation visible in Figures 2b–2d. These regional differences can likely be partially attributed to the influence of the Inter-Tropical Convergence Zone (ITCZ), and the El Niño–Southern Oscillation (ENSO), which is a dominant mode of climate variability in the equatorial regions. ENSO, with its periodic shifts in sea surface temperatures and atmospheric pressure across the tropical Pacific, induces substantial interannual variability in temperature and humidity profiles. Most radiative kernels in ClimKern were derived from only 1 year of model output, potentially limiting their ability to capture ENSO-related variations. For instance, kernels based on years with strong El Niño or La Niña events might exhibit different sensitivities compared to those based on more neutral years, leading to a larger spread in the calculated Planck and water vapor feedbacks when applied to the forced climate change scenario. It is important to note that although ENSO can produce regional differences among kernels, this signal does not manifest in global averages (H. Huang & Huang, 2023). Following the same logic, the ITCZ, characterized by deep convection and strong vertical gradients in temperature and moisture, exhibits a notable bias in climate models (Lin, 2007; Tian & Dong, 2020). Therefore, when radiative kernels are derived from climate model base states rather than reanalysis data, they may exhibit different sensitivities to temperature.

Soden et al. (2008) showed that kernels from different models differ due to both the radiative transfer code and the base state. Furthermore, while Pincus et al. (2020) have evaluated line-by-line radiative transfer models and found them to contribute little to the spread, climate models actually employ broadband parameterized radiative transfer codes to develop kernels. Therefore, the differences across kernels stem partly from the varying broadband radiative transfer codes and, more importantly, from the base state from which the radiative perturbations are computed and then used in kernel construction. It is difficult to directly examine the influence of different base states in existing radiative kernel sets. The first climate-model-derived kernels are approaching 20 years old, making the simulations used to generate them difficult to locate, if they still exist at all (Shell et al., 2008; Soden & Held, 2006; Soden et al., 2008). Furthermore, papers documenting new sets of kernels often do not provide sufficient detail to replicate the simulations themselves. However, we can use the fact that observation-derived kernels are often generated using similar, even overlapping, observational records. For example, of the three

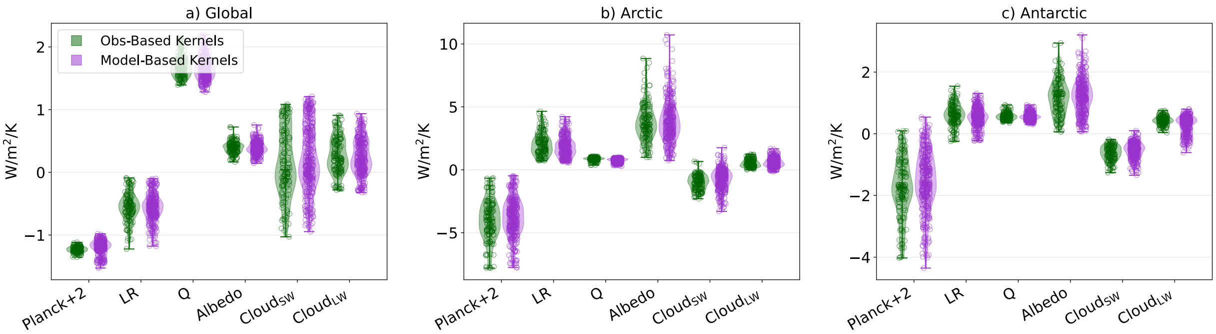

Figure 3. Distributions of feedback parameters across the full sample of kernel–model combinations, shown separately for kernels derived from observational data sets (green; 3 kernels × 48 models = 144 values) and climate model simulations (purple; 7 kernels × 48 models = 336 values). Each violin shows the kernel density of the sample, with the median and full range marked; overlaid points show the individual values. Distributions are shown for (a) global, (b) Arctic, and (c) Antarctic regions. Observation-based kernels exhibit less variability than model-based kernels. Table S2 in Supporting Information S1 provides more information about each kernel.

observation-based kernels used in this study, the years included to derive the kernels are 2008–2012 for ECMWF-RRTM (Y. Huang et al., 2017), 2011–2015 for ERA5 (H. Huang & Huang, 2023), and 2008 for CERES (Thorsen et al., 2018). It is important to note that both the ECMWF-RRTM and ERA5 kernels are derived using the same underlying ECMWF reanalysis data. Thus, these observation-based kernels not only cover a period of similar radiative forcing but were also derived from base states that are significantly more similar than the wide variety of mean states found across climate-model-derived kernels.

To examine the influence of base state on interkernel spread, we categorize the kernels as observation-based (green in Figure 3) or climate-model-based (purple in Figure 3). We find that, for both global means (panel a) and polar averages (b and c), kernels derived from observational base states in general exhibit a smaller spread than those derived from model base states. This is especially evident for the albedo and cloud feedbacks over the polar regions, where observational kernels show minimal spread, with most of the variability driven by model-based kernels. While this basic classification underscores the influence of base-state choice on interkernel spread, a more detailed investigation, beyond the scope of this study, is needed to fully identify and understand the sources of interkernel variability.

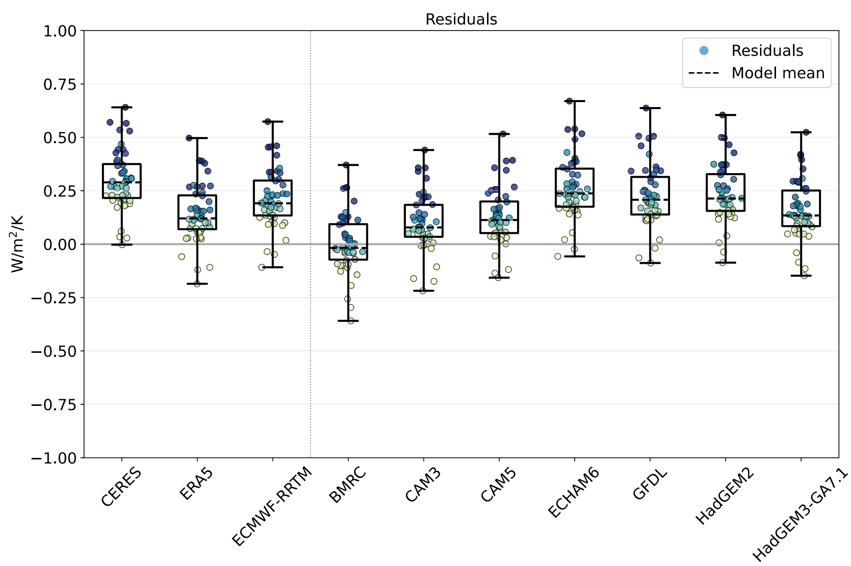

Figure 4. The residuals for each kernel, shown for all 48 models (each model is a different color). The residuals are calculated from subtracting the sum of the individual feedbacks calculated from each kernel from the net radiative feedback parameter calculated as the slope from linearly regressing net top-of-atmosphere radiation and surface temperature response for the 150-year abrupt-4×CO_2 runs for each of the 48 models.

10.1029/2026GL125170

We next assess the intermodel spread of the residuals across the 10 radiative kernels (Figure 4). These residuals—defined as the difference between the net feedback parameter (λ) computed directly from model output and the sum of kernel-derived individual feedbacks—quantify deviations from the linear decomposition assumption. We find that the intermodel spread of these residuals is remarkably similar across all kernels, spanning a range of 0.7 Wm^{-2}. While some kernels (e.g., BMRC, ERA5) have multi-model mean residuals closer to zero than others (e.g., HadGEM2), the relative intermodel ranking for individual models (dots) remains highly consistent across all kernels, a feature also noted in previous studies (Zelinka et al., 2020). To illustrate this consistent ordering, we assign each climate model a unique color shade from yellow to blue. Models with large residuals for one kernel systematically exhibit similarly large residuals for all other kernels, as indicated by the tight vertical alignment of these colors across the boxplots. Because this residual structure reflects the degree to which individual climate models deviate from the linear feedback assumption, rather than the choice of diagnostic kernel, a kernel with a smaller mean residual merely shifts the bias distribution without correcting the underlying non-linearities. Hence, it is misleading to identify a single "best" kernel, and we refrain from recommending one.

4. Discussion and Conclusion

We investigated the choice of radiative kernel and found it to be an important yet often overlooked source of uncertainty in radiative feedback analysis. By applying 10 distinct kernels to the output from abrupt-4×CO_2 experiments across 48 CMIP5 and CMIP6 climate models, we quantified the interkernel spread in globally averaged individual feedback estimates and found it substantial, especially for the Planck, water vapor, and albedo feedbacks. This kernel-induced uncertainty is even more pronounced in the polar regions, where the spread across kernels can match that across models for SW cloud feedbacks. Our analysis further suggests that differences in the base climate state used to derive each kernel are a primary driver of interkernel variability. Additionally, the residuals between the net feedback and the sum of kernel-derived components show intermodel variability comparable to that of the net feedback itself.

An important source of the interkernel spread may be the assumption of linearity when decomposing the net feedback parameter into individual feedbacks using kernels. This assumption enables the use of radiative kernels to isolate feedback components but neglects potential overlap between them. One area where this overlap is particularly evident is between the surface albedo and SW cloud feedbacks, for which we found a large interkernel spread relative to the intermodel spread. In fact, the largest interkernel to intermodel spread occurs along the sea-ice edge regions of the Southern Ocean and the Arctic, suggesting that feedback overlap in these areas contributes to kernel-related uncertainty. Beyond the challenge of separating feedbacks cleanly with feedbacks, previous studies have shown that the linearity assumption also neglects non-linear interactions between the feedbacks themselves, particularly at local scales (Bonan et al., 2025; Feldl & Roe, 2013; Feldl et al., 2017; Y. Huang et al., 2021; Knutti & Rugenstein, 2015). Moreover, feedbacks themselves are not fixed but vary with the state of the climate, such as the spatial pattern of surface temperature change (Armour et al., 2024; Dong et al., 2019; Gregory & Andrews, 2016; Knutti & Rugenstein, 2015; Meyssignac et al., 2023).

We find that kernels based on observational data have lower interkernel spread than those derived from model data (Figure 3). This difference likely arises because the kernels depend on the mean state from which they are derived, as shown in previous studies (H. Huang & Huang, 2023; Pincus et al., 2020), and observationally based kernels likely have more similar base states than the mean states derived from various models. Further work is needed to clarify the criteria for kernel selection in climate feedback studies.

In addition to the more traditional feedback framework we utilized for this study, one could also quantify the effect of warming and moistening at constant relative humidity, as described in the framework of Held and Shell (2012). In that framework, some of the spread in LR and water vapor feedback would likely be reduced, as these components are treated together rather than separately. Future work could explore how interkernel differences manifest under this alternative formulation.

Our findings have practical implications for studies that rely on multi-model comparisons of radiative feedbacks. At the global scale, the intermodel variance is nearly independent of the chosen kernel (Figure S5a in Supporting Information S1). However, at high latitudes, the per-kernel intermodel variance directly affects the overall intermodel spread, most prominently for the albedo and Planck feedbacks (Figures S5b and S5c in Supporting Information S1). The substantial inter-kernel spread in polar regions suggests that our process-level understanding of polar amplification is less constrained than multi-model ensembles alone might imply. If diagnostic tools cannot reliably partition the contributions of albedo and cloud processes, it complicates efforts to apply observational constraints to model projections. Given that kernel-induced uncertainty is comparable to the intermodel spread for certain feedbacks and regions, particularly in the high latitudes, caution is warranted when interpreting or comparing feedback strengths across models. Studies focused on polar amplification or other regional feedbacks may especially benefit from conducting sensitivity tests with multiple kernels to evaluate the robustness of their conclusions.

Conflict of Interest

The authors declare no conflicts of interest relevant to this study.

Availability Statement

The ClimKern kernel and data repository is available from Janoski et al. (2026), and is described in Janoski et al. (2025). The CMIP5 and CMIP6 data can be downloaded from the Earth System Grid Federation (ESGF) website at https://esgf-node.llnl.gov/projects/esgf-llnl/.

Acknowledgments
KW was supported by a summer undergraduate internship from the High Meadows Environmental Institute at Princeton University. IM is supported by a Harry Hess postdoctoral fellowship from the Geosciences department at Princeton University. GV was supported by a Grant from the Simons Foundation (MPS-SRM-00006584).

References

Armour, K. C., Proistosescu, C., Dong, Y., Hahn, L. C., Blanchard-Wrigglesworth, E., Pauling, A. G., et al. (2024). Sea-surface temperature pattern effects have slowed global warming and biased warming-based constraints on climate sensitivity. *Proceedings of the National Academy of Sciences*, *121*(12), e2312093121. https://doi.org/10.1073/pnas.2312093121

Bonan, D. B., Kay, J. E., Feldl, N., & Zelinka, M. D. (2025). Mid-latitude clouds contribute to arctic amplification via interactions with other climate feedbacks. *Environmental Research: Climate*.

Charney, J. G., Arakawa, A., Baker, D. J., Bolin, B., Dickinson, R. E., Goody, R. M., et al. (1979). *Carbon dioxide and climate: A scientific assessment*. National Academy of Sciences.

Chung, E.-S., & Soden, B. J. (2015). An assessment of direct radiative forcing, radiative adjustments, and radiative feedbacks in coupled ocean–atmosphere models. *Journal of Climate*, *28*(10), 4152–4170. https://doi.org/10.1175/JCLI-D-14-00436.1

Curry, J. A., Schramm, J. L., & Ebert, E. E. (1995). Sea ice-albedo climate feedback mechanism. *Journal of Climate*, *8*(2), 240–247. https://doi.org/10.1175/1520-0442(1995)008<0240:siacfm>2.0.co;2

Dong, Y., Proistosescu, C., Armour, K. C., & Battisti, D. S. (2019). Attributing historical and future evolution of radiative feedbacks to regional warming patterns using a green's function approach: The preeminence of the western pacific. *Journal of Climate*, *32*(17), 5471–5491. https://doi.org/10.1175/JCLI-D-18-0843.1

Donohoe, A., Blanchard-Wrigglesworth, E., Schweiger, A., & Rasch, P. J. (2020). The effect of atmospheric transmissivity on model and observational estimates of the sea ice albedo feedback. *Journal of Climate*, *33*(13), 5743–5765. https://doi.org/10.1175/JCLI-D-19-0674.1

Feldl, N., Bordoni, S., & Merlis, T. M. (2017). Coupled high-latitude climate feedbacks and their impact on atmospheric heat transport. *Journal of Climate*, *30*(1), 189–201. https://doi.org/10.1175/jcli-d-16-0324.1

Feldl, N., & Roe, G. H. (2013). The nonlinear and nonlocal nature of climate feedbacks. *Journal of Climate*, *26*(21), 8289–8304. https://doi.org/10.1175/jcli-d-12-00631.1

Gregory, J. M., & Andrews, T. (2016). Variation in climate sensitivity and feedback parameters during the historical period. *Geophysical Research Letters*, *43*(8), 3911–3920. https://doi.org/10.1002/2016gl068406

Gregory, J. M., Ingram, W. J., Palmer, M. A., Jones, G. S., Stott, P. A., Thorpe, R. B., et al. (2004). A new method for diagnosing radiative forcing and climate sensitivity. *Geophysical Research Letters*, *31*(3). https://doi.org/10.1029/2003GL018747

Hahn, L. C., Armour, K. C., Zelinka, M. D., Bitz, C. M., & Donohoe, A. (2021). Contributions to polar amplification in cmip5 and cmip6 models. *Frontiers in Earth Science*, *9*, 710036. https://doi.org/10.3389/feart.2021.710036

He, H., Kramer, R. J., Soden, B. J., & Jeevanjee, N. (2023). State dependence of co_2 forcing and its implications for climate sensitivity. *Science*, *382*(6674), 1051–1056. https://doi.org/10.1126/science.abq6872

Held, I. M., & Shell, K. M. (2012). Using relative humidity as a state variable in climate feedback analysis. *Journal of Climate*, *25*(8), 2578–2582. https://doi.org/10.1175/JCLI-D-11-00721.1

Huang, H., & Huang, Y. (2023). Radiative sensitivity quantified by a new set of radiation flux kernels based on the ecmwf reanalysis v5 (era5). *Earth System Science Data*, *15*(7), 3001–3021. https://doi.org/10.5194/essd-15-3001-2023

Huang, Y., Huang, H., & Shakirova, A. (2021). The nonlinear radiative feedback effects in the arctic warming. *Frontiers in Earth Science*, *9*, 693779. https://doi.org/10.3389/feart.2021.693779

Huang, Y., Xia, Y., & Tan, X. (2017). On the pattern of co2 radiative forcing and poleward energy transport. *Journal of Geophysical Research: Atmospheres*, *122*(20), 10–578. https://doi.org/10.1002/2017JD027221

Huo, Y., Wang, H., Lu, J., Fu, Q., Jonko, A. K., Lee, Y. J., et al. (2024). Assessing radiative feedbacks and their contribution to the arctic amplification measured by various metrics. *Journal of Geophysical Research: Atmospheres*, *129*(21), e2024JD040880. https://doi.org/10.1029/2024JD040880

Janoski, T. P., Mitevski, I., & Kramer, R. J. (2026). ClimKern kernel and data repository (version 1.2.1) [Dataset]. *Zenodo*. https://doi.org/10.5281/zenodo.18565513

Janoski, T. P., Mitevski, I., Kramer, R. J., Previdi, M., & Polvani, L. M. (2025). Climkern v1. 2: A new python package and kernel repository for calculating radiative feedbacks. *Geoscientific Model Development*, *18*(10), 3065–3079. https://doi.org/10.5194/gmd-18-3065-2025

Knutti, R., & Rugenstein, M. A. (2015). Feedbacks, climate sensitivity and the limits of linear models. *Philosophical Transactions of the Royal Society A: Mathematical, Physical and Engineering Sciences*, *373*(2054), 20150146. https://doi.org/10.1098/rsta.2015.0146

Lin, J.-L. (2007). The double-itcz problem in ipcc ar4 coupled gcms: Ocean–atmosphere feedback analysis. *Journal of Climate*, *20*(18), 4497–4525. https://doi.org/10.1175/jcli4272.1

10.1029/2026GL125170

Meyssignac, B., Chenal, J., Loeb, N., Guillaume-Castel, R., & Ribes, A. (2023). Time-variations of the climate feedback parameter λ are associated with the pacific decadal oscillation. *Communications Earth & Environment*, *4*(1), 241. https://doi.org/10.1038/s43247-023-00887-2

Mitevski, I., Polvani, L. M., He, H., Vecchi, G. A., Orbe, C., Soden, B. J., & Miller, R. L. (2025). State dependence of co2 effective radiative forcing from 1/16× to 16× CO_2. *Journal of Climate*, *38*(19), 5323–5333. https://doi.org/10.1175/JCLI-D-24-0387.1

Pincus, R., Buehler, S. A., Brath, M., Crevoisier, C., Jamil, O., Franklin Evans, K., et al. (2020). Benchmark calculations of radiative forcing by greenhouse gases. *Journal of Geophysical Research: Atmospheres*, *125*(23), e2020JD033483. https://doi.org/10.1029/2020jd033483

Riihelä, A., Bright, R. M., & Anttila, K. (2021). Recent strengthening of snow and ice albedo feedback driven by antarctic sea-ice loss. *Nature Geoscience*, *14*(11), 832–836. https://doi.org/10.1038/s41561-021-00841-x

Shell, K. M., Kiehl, J. T., & Shields, C. A. (2008). Using the radiative kernel technique to calculate climate feedbacks in ncar's community atmospheric model. *Journal of Climate*, *21*(10), 2269–2282. https://doi.org/10.1175/2007JCLI2044.1

Sherwood, S. C., Webb, M. J., Annan, J. D., Armour, K. C., Forster, P. M., Hargreaves, J. C., et al. (2020). An assessment of earth's climate sensitivity using multiple lines of evidence. *Reviews of Geophysics*, *58*(4), e2019RG000678. https://doi.org/10.1029/2019RG000678

Soden, B. J., Collins, W. D., & Feldman, D. R. (2018). Reducing uncertainties in climate models. *Science*, *361*(6400), 326–327. https://doi.org/10.1126/science.aau1864

Soden, B. J., & Held, I. M. (2006). An assessment of climate feedbacks in coupled ocean–atmosphere models. *Journal of Climate*, *19*(14), 3354–3360. https://doi.org/10.1175/jcli3799.1

Soden, B. J., Held, I. M., Colman, R., Shell, K. M., Kiehl, J. T., & Shields, C. A. (2008). Quantifying climate feedbacks using radiative kernels. *Journal of Climate*, *21*(14), 3504–3520. https://doi.org/10.1175/2007jcli2110.1

Thorsen, T. J., Kato, S., Loeb, N. G., & Rose, F. G. (2018). Observation-based decomposition of radiative perturbations and radiative kernels. *Journal of Climate*, *31*(24), 10039–10058. https://doi.org/10.1175/JCLI-D-18-0045.1

Tian, B., & Dong, X. (2020). The double-itcz bias in cmip3, cmip5, and cmip6 models based on annual mean precipitation. *Geophysical Research Letters*, *47*(8), e2020GL087232. https://doi.org/10.1029/2020gl087232

Zelinka, M. D., Myers, T. A., McCoy, D. T., Po-Chedley, S., Caldwell, P. M., Ceppi, P., et al. (2020). Causes of higher climate sensitivity in cmip6 models. *Geophysical Research Letters*, *47*(1), e2019GL085782. https://doi.org/10.1029/2019GL085782

Zhang, R., Wang, H., Fu, Q., Pendergrass, A. G., Wang, M., Yang, Y., et al. (2018). Local radiative feedbacks over the arctic based on observed short-term climate variations. *Geophysical Research Letters*, *45*(11), 5761–5770. https://doi.org/10.1029/2018GL077852

Zhang, R., Wang, H., Fu, Q., & Rasch, P. J. (2020). Assessing global and local radiative feedbacks based on agcm simulations for 1980–2014/2017. *Geophysical Research Letters*, *47*(12), e2020GL088063. https://doi.org/10.1029/2020GL088063